Eng. Sci., 2025, **38**, 1908

Engineered Science
DOI: https://dx.doi.org/10.30919/es1908

Novel Ceramic Ultrasonic Horn Ensures Vibration Stability up to 800 °C

Hong Luo,[1,2,#,*] Haitao Zhao,[1,2,#] Xianglong Yang,[1,2] Shuai Ma,[1,2] Xinran Dong,[1] Qingyi Yan,[1] Yang Liu[1] and Zhen Yin[3,*]

Abstract

Ultrasonic horns, serving as the terminal tools for vibration amplification, have been widely used in thermal processes. However, traditional metallic horns suffer from material degradation and thermal deformation at high temperatures, leading to frequency drift and system instability. To address this limitation, this study presented the design of a novel Al_2O_3 ceramic horn to improve the thermal stability of the ultrasonic system. The Al_2O_3 horn was designed based on longitudinal wave theory and fabricated by pressure less sintering. Finite element modal analysis indicated that as the terminal temperature increased from 25 °C to 800 °C, the Al_2O_3 horn's eigenfrequency decreased by only 238 Hz, far lower than the 982-Hz drop in Ti-6Al-4V horn. Experimental modal analysis further confirmed the overall stability of resonant frequency and amplitude of the Al_2O_3 horn over 25–800 °C. The practical performance of the Al_2O_3 horn was evaluated in ultrasonic-assisted micro-embossing of PMMA under 2.45-GHz microwave heating, where high-aspect-ratio, well-defined micro-protrusions were successfully fabricated. The average PMMA-to-mold filling ratio reached 96.79%, 10.72% higher than that of conventional embossing. With its thermal duration and electrical insulation, the designed ceramic horn will unlock the application of high-power ultrasonic systems in extreme environments, particularly those involving high temperatures or intense-electromagnetic fields.

Keywords: Ultrasonic vibration; A_2O_3 ceramic horn; High temperature; Resonant characteristics; Hot embossing.
Received: 17 July 2025; Revised: 28 October 2025; Accepted: 09 November 2025
Article type: Research article.

1. Introduction

Ultrasonic vibration systems, which convert electrical energy into high-frequency mechanical oscillation, have been widely used in melt treatment,[1] embossing/casting,[2,3] and advanced welding applications.[4] As the key terminal tool, the ultrasonic horn (also sonotrode) plays a crucial role in energy focusing and amplitude amplification.[5] However, conventional metallic horns (*e.g.* aluminum alloys) are prone to material degradation and thermal deformation at high temperatures, leading to undesirable frequency drift (>1000 Hz drop at 600 °C)[6] and system detuning. This thermo-mechanical instability has been a common concern in high-power ultrasonic vibration systems.[6,7] Therefore, developing thermally stable horns is crucial for enhanced reliability of ultrasonic systems in advanced thermal processes.

The development of ultrasonic horns primarily focuses on structural design and material innovation. Regarding structural design, Kuma *et al*.[8] introduced longitudinal grooves to the horn, which reduced local heat accumulation and improved plastic welding efficiency by 20%. Tsai *et al*.[9] compensated for the reduction in eigenfrequency at elevated temperatures by shortening the horn's length, thus extending the horn's maximum operating temperature from 250 °C to 450 °C. Liu *et al*.[10] further employed finite element method (FEM) and genetic algorithm to dimensionally optimize the multi-stepped horn, specifically addressing the eigenfrequency drift of the ultrasonic oscillator in laser welding. Despite these advancements, there are inherent limitations in relying solely geometric adjustments to achieve high-temperature stability of the ultrasonic system.

In terms of material selection for ultrasonic horns, commonly used options include aluminum alloys,[11] alloy/carbon steels,[12] and titanium alloys,[6] each demonstrating distinct characteristics (Table 1). Aluminum

---

[1] *College of Mechanical and Intelligent Manufacturing, Central South University of Forestry and Technology, Changsha, 410004, China*
[2] *Engineering Research Center for Forestry Equipment of Hunan Province, Central South University of Forestry and Technology, Changsha, 410004, China*

Table 1: Performances and applications of ultrasonic horns made of different materials.

Horn material	Mechanical strength	Thermal stability	Acoustic efficiency	Cost efficiency	Typical application
Aluminum alloys	Low	Low	Moderate	High	Plastic welding,[13] ultrasonic insertion[14]
Alloy/carbon steels	High	Moderate	Low	Moderate	Mechanical machining,[19] hot embossing[20]
Titanium alloys	Moderate	Moderate	High	Low	Glass molding,[21] ultrasonic comminution[22]

alloy horns are widely used in plastic welding[13] and ultrasonic insertion[14] owing to their superior acoustic characteristics and cost efficiency, yet their mechanical strength and thermal stability are limited. Alloy/carbon steel horns offer enhanced mechanical strength and thermal stability, but their high acoustic impedance may induce excessive energy loss and heat accumulation.[16] Overall, titanium alloy horns, combining high strength, high thermal stability, and low acoustic impedance, are favored in high-temperature/high-power applications.[17] For example, a Ti-6Al-4V horn by Song *et al*.[15] maintained stable operation in 180 °C oil baths, while Liu *et al*.[10] reported a titanium horn capable of operating at up to 377 °C during laser welding. Notably, Yu *et al*.[6] developed a Ti-6Al-4V horn for glass molding, and the maximum operating temperature reached 641 °C. Despite these advances, metallic materials, including titanium alloys, are inherently thermally sensitive. At elevated temperatures, they undergo substantial changes in material properties and thermal expansion, leading to undesirable frequency drift and system detuning.[6] In contrast, ceramic materials offer a potential alternative due to their low thermal expansion and excellent thermal duration.[16] Furthermore, ceramics generally offer superior chemical stability and electrical insulation, ensuring reliable performance even in extreme environments involving corrosive media or strong electromagnetic fields - conditions where metallic horns are susceptible to oxidation, corrosion, or electromagnetic interference. Although the use of SiAlON and Si_3N_4 ceramics in ultrasonic horns for molten alloy solidification has been reported in limited studies,[17,18] there is a significant lack of methodological research into the analytical design of ceramic horns and comprehensive characterization of their high-temperature performance.

To bridge the above gap, this study introduces a comprehensive framework for the design, characterization, and application of a novel ceramic horn, offering a viable approach for the development of high-temperature ultrasonic systems. First, a typical cylindrical Al_2O_3 horn was designed based on longitudinal wave theory. FEM modal analysis was then conducted to investigate the resonant characteristics of the Al_2O_3 coupled ultrasonic oscillator. Additionally, experimental modal analysis was performed to validate the vibration stability of the Al_2O_3 horn at elevated temperatures. Finally, the practical performance of the Al_2O_3 horn was assessed through ultrasonic-assisted micro-embossing of PMMA under 2.45-GHz microwave heating. The developed ceramic horn will contribute to advancing the application of ultrasonic technology in harsh operational environments.

2. Theoretical design

2.1 Design of ultrasonic horn

To ensure generality, the typical cylindrical horn is selected as the design case. Considering the requirements for total length adjustment and disassembly, three horn segments are specified, as shown in Fig. 1. The first horn, made of AISI D2 tool steel, connects to the transducer at the origin point *O*, with a mounting flange at its nodal plane. The second horn, made of AISI 316L stainless steel, is thread-connected to the first horn for easy disassembly. The third horn, made of Al_2O_3 ceramic (pressure less-sintered at 1500 °C), is adhesively bonded to the second horn. Material properties for the three horns at room temperature (25 °C) are obtained from the COMSOL material library,[23] as listed in Table 2.

To calculate the theoretical resonant length of the ultrasonic horn at room temperature, the governing equation for longitudinal wave propagation in a

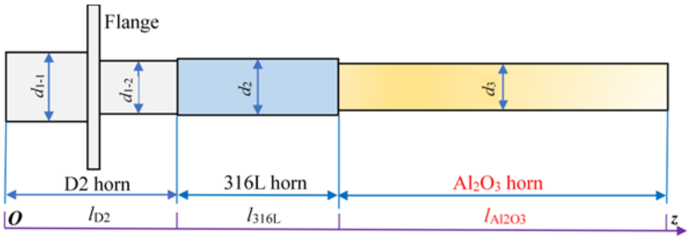

Fig. 1: Geometries of three-stepped cylindrical horn.

---

[3]*College of Mechanical Engineering, Suzhou University of Science and Technology, Suzhou, 215009, China*
[#]*These authors contributed to this work equally.*
[*]*Email:* luohong2017@hnu.edu.cn (Hong Luo),
yinzhen12@usts.edu.cn (Zhen Yin)

Table 2: Physical properties of different horn materials at room temperature (25 °C).

Material	Young's modulus *E* (GPa)	Density (kg/m^3)	Wave velocity (m/s)	Wavelength (mm)
D2	209.82	7693.85	5222.17	267.80
316L	193.43	7967.09	4927.33	252.68
Al_2O_3	392.33	3989.35	9916.92	508.56

homogeneous slender rod is employed:[24]

$$\frac{\partial}{\partial z}\left[AE\frac{\partial u(z,t)}{\partial z}\right]dz = A\rho\frac{\partial^2 u(z,t)}{\partial t^2}dz \qquad (1)$$

where t is time, ρ and E are the density and Young's modulus, A is the cross-sectional area of the rod, and $u(z, t)$ denotes the longitudinal displacement at position z.

By solving Eq. (1), the theoretical resonant length l of the horn under free vibration can be derived as:

$$l = \frac{i}{2f}\sqrt{E/\rho} = \frac{i}{2f}v = i\frac{\lambda}{2}, \quad (i \in \mathbb{N}^+) \qquad (2)$$

where i is a positive integer, f is the design frequency, and v and λ are the wave speed and wavelength in the horn, respectively.

As indicated in Eq. (2), the resonant length of each horn (Fig. 1) is an integer multiple of $\lambda/2$. For $i = 1$ and $f = 19.5$ kHz, the resonant lengths are calculated as $l_{D2} = 133.90$ mm for the D2 horn, $l_{316L} = 126.34$ mm for the 316L horn, and $l_{Al2O3} = 254.28$ mm for the Al_2O_3 horn. To suppress transverse vibration, the diameter of each horn should be less than a quarter wavelength ($\lambda/4$).[6] Based on this design criterion, the rear-end and front-end diameters of the D2 horn are set as $d_{1,1} = 54$ mm and $d_{1,2} = 31$ mm, respectively. The diameters of the 316L and Al_2O_3 horns are set as $d_2 = 32$ mm and $d_3 = 30$ mm, respectively.

2.2 Design of piezoelectric transducer

The ultrasonic transducer serves as an essential component in ultrasonic systems by converting alternating current into high-frequency mechanical vibration.[25,26] This study employs the most commonly sandwiched piezoelectric transducer, as shown in Fig. 2. Its core piezoelectric stack consists of four parallel-connected PZT-8 ceramic rings, which are suitable for high-power applications. Each PZT-8 ring has an outer diameter of 50 mm, inner diameter of 14.5 mm, and thickness of 6.0 mm. To enhance forward acoustic radiation efficiency, the transducer incorporates a graded density design: the rear cover is made of high-density AISI 1045 steel while the front cover is made of low-density AISI 2024 aluminum alloy, both with a diameter of 50 mm. An M12 steel bolt (AISI 1045 steel) was used to apply axial preload to the PZT-8 stack, maintaining compressive stress that prevents cracking during vibration. The material properties of each part of the transducer are listed in Table 3, according to the COMSOL built-in material library.

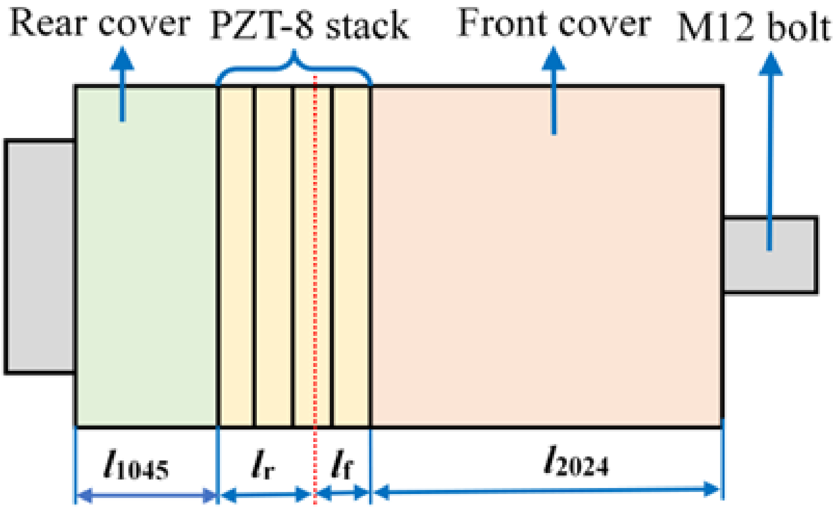

Fig. 2: Schematic view of sandwiched piezoelectric transducer.

Table 3: Materials properties of piezoelectric transducer parts.

Part (material)	Young's modulus (GPa)	Density (kg/m^3)	Poisson's ratio	Wave velocity (m/s)	Angle wave velocity at 19.5 kHz (rad/m)	Wavelength at 19.5 kHz (mm)
Rear cover (1045 steel)	212.19	7858.94	0.29	5196.12	23.58	266.47
Ceramic stack (PZT-8)	123.00	7600.00	0.23	4022.96	30.46	206.31
Front cover (2024 Al alloy)	72.96	2779.18	0.33	5123.84	23.91	262.76

According to the principle of electro-mechanical equivalent circuit,[12,19] to ensure efficient coupling between the mechanical and electrical characteristics of the ultrasonic transducer, the lengths of the rear and front covers should satisfy the following frequency equations:

$$tan(k_{1045}l_{1045}) = \frac{\rho_{\mathrm{pzt}}v_{\mathrm{pzt}}S_{\mathrm{pzt}}}{\rho_{1045}C_{1045}S_{1045}}cot(k_{\mathrm{pzt}}l_r) \qquad (3)$$

$$tan(k_{2024}l_{2024}) = \frac{\rho_{\mathrm{pzt}}v_{\mathrm{pzt}}S_{\mathrm{pzt}}}{\rho_{2024}C_{2024}S_{2024}}cot(k_{\mathrm{pzt}}l_f) \qquad (4)$$

where l_{r} and l_{f} are the lengths of the PZT-8 stack on the rear and front sides of the wave node; k_{pzt}, ρ_{pzt}, v_{pzt}, and S_{pzt} are the angular wavenumber, density, wave velocity, and cross-sectional area of the PZT-8 ceramic, respectively; l_{1045}, k_{1045}, ρ_{1045}, C_{1045}, S_{1045} are the length, angular wavenumber, density, wave velocity, and cross-sectional area of the rear cover, respectively; l_{2024}, k_{2024}, ρ_{2024}, C_{2024}, S_{2024} are the length, angular wavenumber, density, wave velocity, and cross-sectional area of the front cover, respectively.

Since the front cover's length can be taken as a quarter wavelength,[27] i.e., l_{2024} = 65.69 mm, the length of the rear cover was calculated as l_{1045} = 28.29 mm, based on Eq. (3) and (4). These theoretical calculations defined the main dimensions of both the transducer and horn, providing the geometric model for subsequent FEM simulations.

3. Numerical simulation

3.1 Modal simulation at room temperature

FEM modal analysis of the Al_2O_3 horn coupled ultrasonic oscillator was conducted using COMSOL Multiphysics software. Five consecutive eigenmodes were identified near the design frequency of 19.5 kHz, as detailed in Table S1 (*Supporting Information file*). A single longitudinal vibration mode was observed at 19.491 kHz (Fig. 3a), which is only 0.46% below the design frequency (19.5 kHz). This close agreement confirms the validity of applying longitudinal wave theory in horn design. The slight frequency discrepancy can be attributed to the theoretical design not accounting for the influence of horn diameter and structural details on the resonant characteristics.

Frequency-domain perturbation analysis of the ultrasonic oscillator was further performed by coupling the electrostatic field and solid mechanics modules. The boundary conditions included fixed constraints at both ends of the mounting flange and a frequency-sweep voltage excitation (19.25–19.75 kHz, 88 V amplitude) applied to the PZT stack's anode, with the cathode grounded (Fig. 3b). The simulation results indicate that when the applied voltage frequency matches the resonant frequency of the ultrasonic oscillator (19.490 kHz), the output amplitude of the Al_2O_3 horn reaches the maximum value of 5.62 µm (Fig. 3c). The displacement amplification factor, calculated by the ratio of output (5.62 µm) to input amplitude (1.61 µm), was determined to be 3.49. The vibration amplitude and amplification factor are sufficient for ultrasonic-assisted micro/nano-machining/forming processes.[28,29]

3.2 Modal simulation at high temperature

To investigate the high-temperature performance of the Al_2O_3 horn, modal analysis of the ultrasonic oscillator was conducted by coupling the Solid Heat Transfer, Solid Mechanics, and Electrostatic modules in COMSOL. Temperature-dependent material properties, well-defined in the COMSOL material library,[23] were assigned to the horn to enhance simulation accuracy. Boundary conditions included fixing both ends of the flange while maintaining 800 °C at the horn tip to replicate sustained high-temperature conditions. After performing

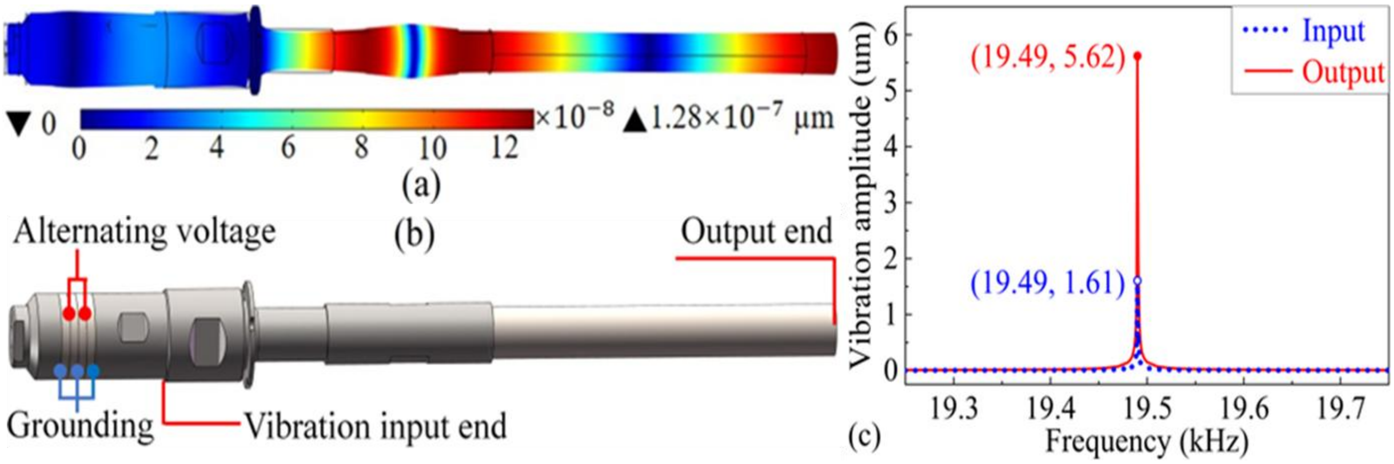

Fig. 3: FEM modal analysis of ultrasonic oscillator coupled with Al_2O_3 horn at room temperature: (a) Mode shape at 19.49 kHz, (b) boundary conditions for frequency-domain perturbation analysis and (c) the obtained Amplitude spectra.

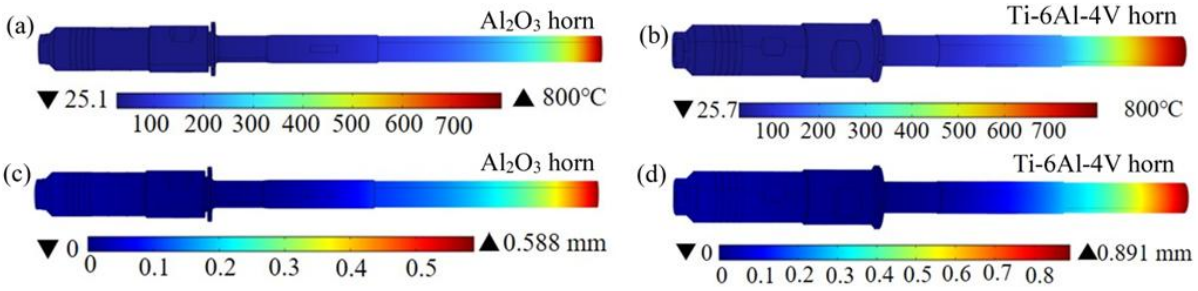

Fig. 4: (a, b) Temperature distributions and (c, d) axial thermal deformations of ultrasonic oscillators coupled with Al_2O_3 horn and (b, d) Ti-6Al-4V horn under 800°C tip heating.

steady-state thermo-mechanical analysis, the temperature distributions and axial thermal deformations of the ultrasonic oscillators coupled with the Al_2O_3 horn and Ti-6Al-4V horn were obtained (Fig. 4). As indicated, both horns develop localized high temperatures under tip heating at 800°C, but the high-temperature zone in the Al_2O_3 horn is smaller than that in the Ti-6Al-4V horn (Fig. 4a and b). This difference can be attributed to the higher specific heat capacity of Al_2O_3 compared to Ti-6Al-4V (Fig. S1a, *Supporting Information file*). Additionally, the axial thermal deformation of the Al_2O_3 horn is observed to be only 0.588 mm, significantly lower than the 0.891 mm expansion for the Ti-6Al-4V horn (Fig. 4c and d). This difference arises from the smaller high-temperature zone and the lower coefficient of thermal expansion of the Al_2O_3 horn (Fig. S1b, *Supporting Information file*). These findings collectively indicate that the designed Al_2O_3 horn exhibits superior thermal stability compared to the typical Ti-6Al-4V horn, making it more suitable for high-temperature applications.

Fig. 5a and b shows the frequency responses of the Al_2O_3 horn and Ti-6Al-4V horn under tip heating at 800 °C, respectively. Both horns exhibit eigenfrequency reduction compared to their room-temperature performance, which is consistent with findings by Yu *et al*.[6] This thermally induced eigenfrequency reduction can be explained by the extended form of Eq. (2):

$$f(T) = i\frac{v(T)}{2l(T)} = i\frac{E(T)^{0.5}\rho(T)^{-0.5}}{2l[1+\alpha(T)(T-T_0)]}, (i \in \mathbb{N}^+) \qquad (5)$$

As indicated in Eq. (5), increasing temperature T reduces the horn's Young's modulus $E(T)$ and density $\rho(T)$ while increasing the horn's length $l(T)$, resulting in decreased longitudinal eigenfrequency $f(T)$. Meanwhile, both horns demonstrate amplitude reduction under 800°C tip heating (Fig. 5), which may be related to the increased damping dissipation at elevated temperatures.[30] It is noteworthy that at 800°C, the longitudinal eigenfrequency of the Ti-6Al-4V horn drops from 19468 Hz (at room temperature) to 18486 Hz, with a reduction of 982 Hz. This substantial frequency drift could degrade the electro-acoustic conversion efficiency and even cause detuning in ultrasonic vibration systems, particularly given the limited bandwidth of industrial PZT transducers and potential excitation of unintended vibration modes.[6,20] In contrast, the Al_2O3 horn experiences only a 238-Hz decrease in frequency at high temperature, and the amplitude decrease (1.61 μm) is significantly lower than that of the Ti-6Al-4V horn (12.55 μm). These results confirm that the Al_2O3 horn can significantly improve both the frequency and amplitude stability of the ultrasonic system operating under high-temperature conditions.

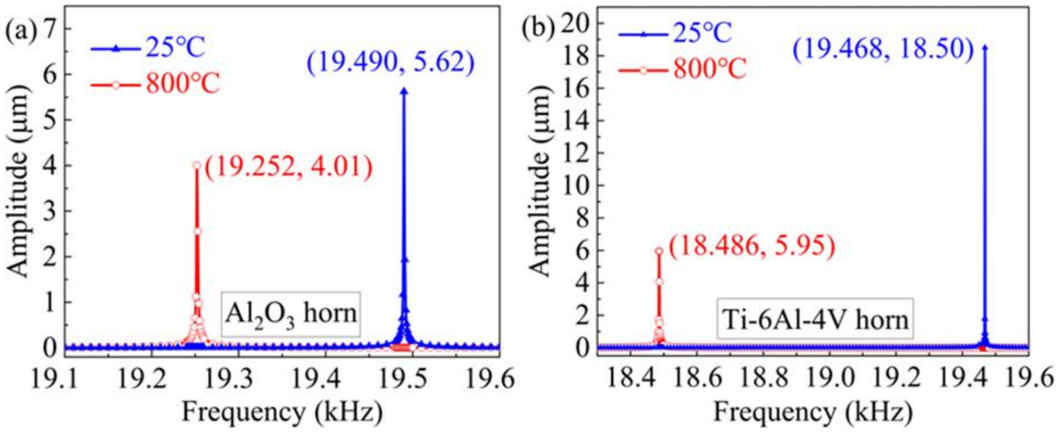

Fig. 5: Amplitude spectra of ultrasonic oscillators coupled with (a) Al_2O_3 horn and (b) Ti-6Al-4V horn at room/high temperatures.

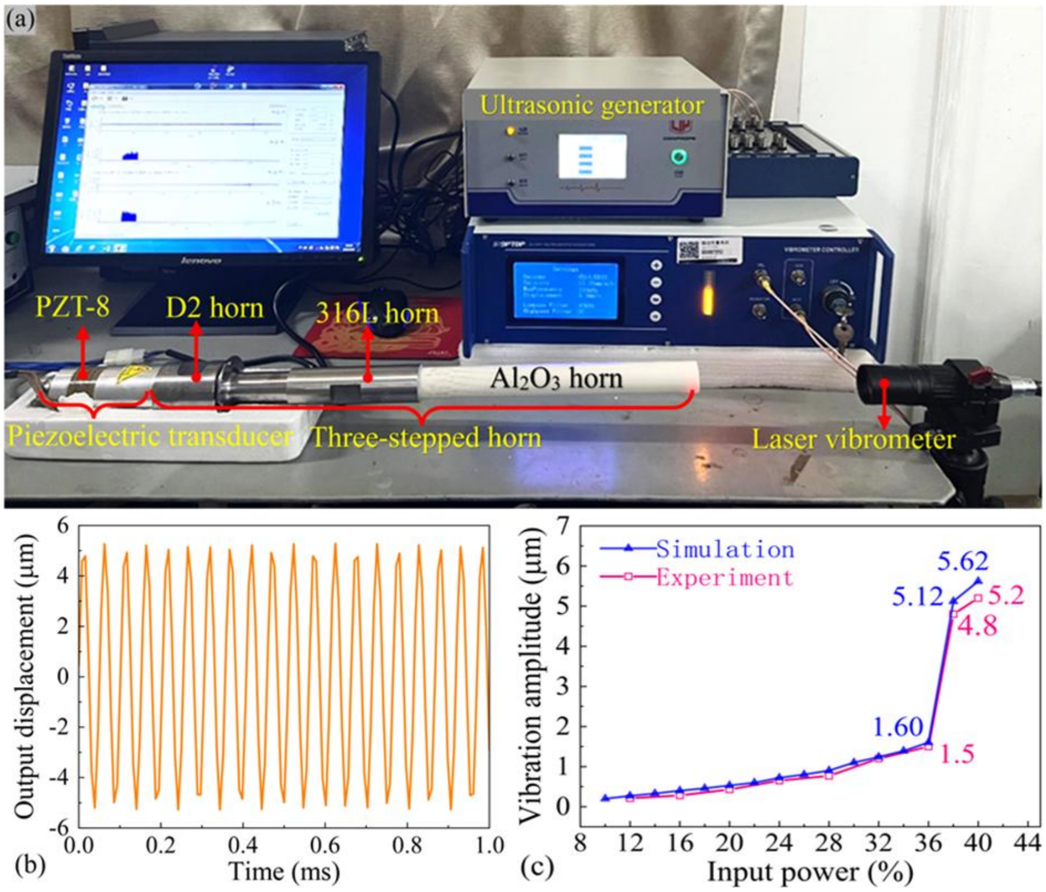

Fig. 6: Experimental modal analysis of ultrasonic oscillator coupled with Al_2O_3 horn: (a) Experimental setup, (b) output displacement at 40% ultrasonic power, and (c) variation of amplitude with ultrasonic power.

4. Experimental validation

4.1 Modal experiment at room temperature

To validate the numerical results, experimental modal analysis was performed on the Al_2O_3 horn-coupled ultrasonic oscillator, as shown in Fig. 6a. To avoid brittle fracture of the Al_2O_3 horn, the applied ultrasonic power was limited to 40%. The output displacement of the horn was measured using a laser vibrometer (LV-SF01, Yuyao Sunny Optical Intelligence Technology Co., Ltd, China), with a maximum linear error of ±1%. A typical periodic vibration signal at the horn's output end, at 40% power, is shown in Fig. 6b. The extracted vibration amplitudes of the Al_2O_3 horn at different power levels are plotted in Fig. 6c. It can be observed that within the 10%–36% power range, the amplitude increases nearly linearly, which is consistent with the observation by Chen *et al*.[31] However, when the power increases from 36% to 38%, a sharp increase in amplitude occurs. This nonlinear trend arises from the unique voltage setting: the voltage increases linearly from 10% to 36% power, but rises sharply between 36% and 38%. This configuration provides a broader range of amplitude adjustment to accommodate varying operating conditions. Notably, at 40% power, the actual vibration amplitude of the Al_2O_3 horn was 5.20 μm (Fig. 6c), which closely matches the FEM-calculated value (5.62 μm), confirming the accuracy of the numerical results.

4.2 Modal experiment at elevated temperatures

To verify the thermal stability of the Al_2O_3 horn, experimental modal analysis of the ultrasonic oscillator was conducted using a self-developed microwave heating system (Fig. 7a). This system employs two 2.45-GHz microwave magnetrons (each with the rated power of 1.5 kW) as heat sources to heat a microwave-absorbing SiC sleeve. The heat generated in the SiC sleeve was then transferred to the Al_2O_3 horn through conduction. A specially-designed anti-interference thermocouple, with a measurement range of 0–1100 °C and measurement uncertainty of ±2 °C, was used to monitor the temperature within the SiC sleeve. Once the probed temperature reached the preset value, the system was maintained at this state for 30 minutes to achieve a relatively stable temperature distribution. Subsequently, the vibration amplitude at the center of the Al_2O_3 horn's tip was measured using the LV-SF01 laser vibrometer, while the admittance characteristics of the ultrasonic oscillator were measured using a commercial impedance analyzer (PV520A, Bandera Electronics Co., Ltd, China).

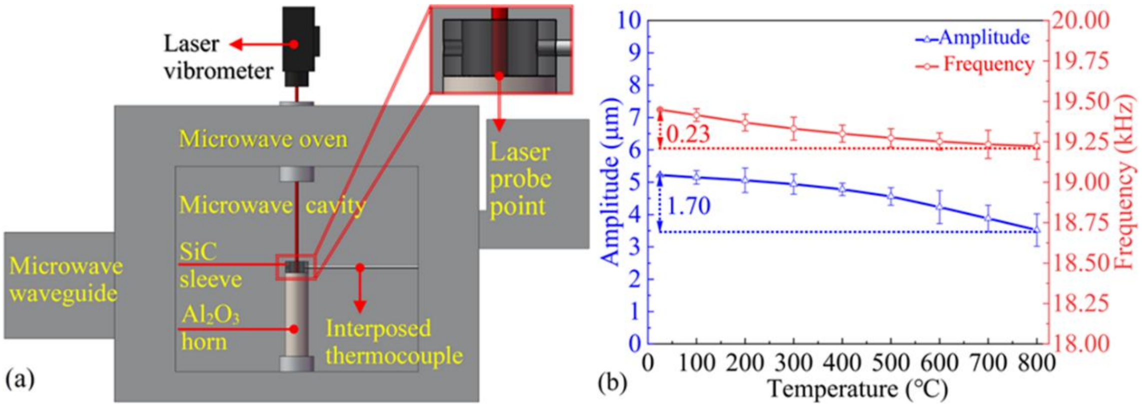

Fig. 7: (a) Schematic view of amplitude measurement of ultrasonic oscillator, and (b) measured amplitudes at elevated temperatures.

Fig. 7b shows the vibration frequencies and amplitudes of the Al_2O_3 horn-coupled ultrasonic oscillator under tip heating at varying temperatures. As the tip temperature increases, both the frequency and amplitude decrease, which aligns with the simulated trend (Fig. 5). It is also noted that the reductions in both parameters remain relatively small, confirming the overall thermal stability of the Al_2O_3 horn. Fig. 8a shows the admittance locus (susceptance-conductance curve) of the ultrasonic oscillator under 800°C tip heating. A typical single circular trajectory is observed without obvious distortions (*e.g.*, sharp protrusions, depressions, or parasitic loops), indicating the well-tuned condition of the resonant system.[6] Furthermore, Fig. 8b demonstrates a single resonant peak P (f_s, G_{max}) within the tested frequency range (18.0–20.5 kHz), and the measured resonant frequency (19.216 kHz) closely matches the FEM-calculated longitudinal eigenfrequency (19.252 kHz) under 800 °C tip heating. This alignment indicates that the Al_2O_3 horn operates in unimodal longitudinal vibration without parasitic modal coupling.[32,33] Notably, the ultrasonic oscillator maintains a high mechanical quality factor (Q_m = 2135) under 800 °C tip heating, indicating low energy loss per cycle.[34] These results collectively confirm the superior frequency/amplitude stability of the Al_2O_3 horn-coupled ultrasonic oscillator under high-temperature conditions, validating the accuracy of the theoretical design and numerical results.

5. Application to ultrasonic-assisted embossing

5.1 Experimental setup

To demonstrate the practical performance of the Al_2O_3 horn under extreme conditions, ultrasonic-assisted PMMA embossing experiments were conducted using the 2.45-GHz microwave heating system (Fig. 7a). Fig. 9a shows the PMMA preform and SiC molds (excluding the insulating sleeve) used in embossing experiments.

The PMMA preform is a cuboid with the size of 14 × 14 × 4 mm^3. The upper and lower molds are cylindrical, each with a diameter of 22 mm and a height of 12 mm. A rectangular microgroove array was fabricated on the lower mold surface through picosecond laser micro-machining (wavelength: 1030 nm, pulse frequency: 500 kHz, laser power: 20 W). The microgrooves have an average top width of 888.63 μm, bottom width of 645.91 μm, depth of 1012.12 μm, and an aspect ratio of 1.14:1. Both molds are made of pressureless-sintered SiC, which can efficiently absorb microwave energy to heat the PMMA preform.[35]

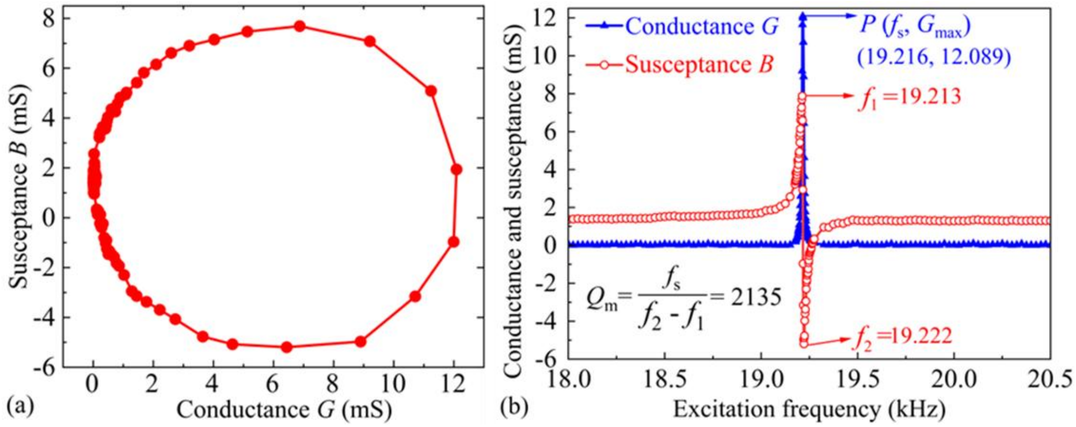

Fig. 8: Measured admittance characteristics of Al_2O_3 horn-coupled ultrasonic oscillator under 800 °C tip heating: (a) Susceptance-conductance curve, and (b) admittance-frequency curve.

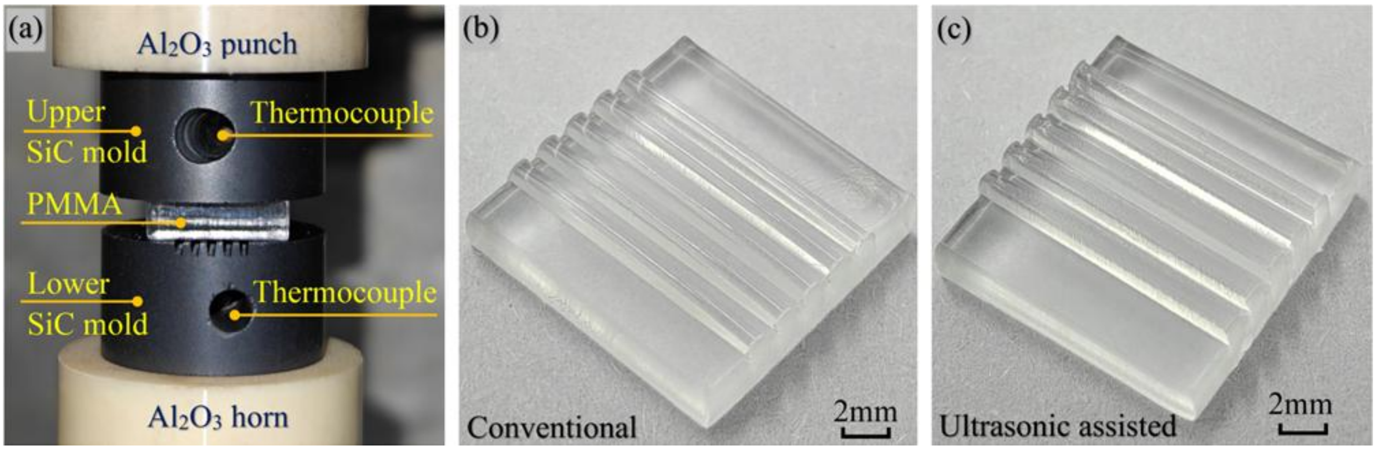

Fig. 9: (a) Experimental details (excluding insulating sleeve), and the replicated PMMA micro-protrusion arrays in (b) conventional and (c) ultrasonic-assisted embossing.

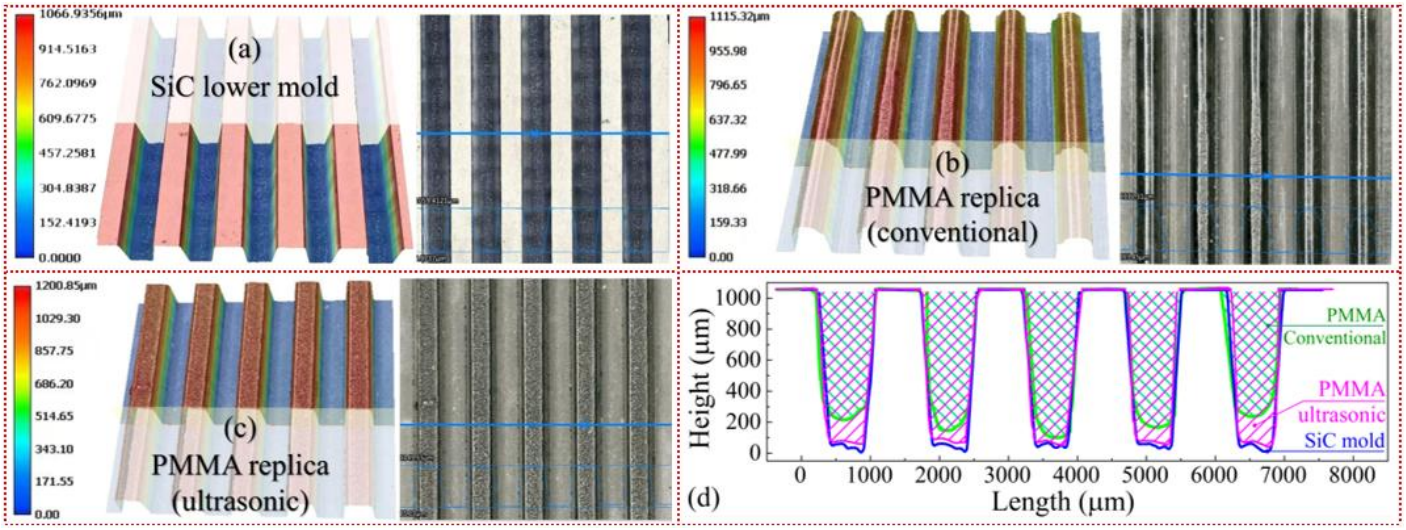

Fig. 10: Surface morphologies of (a) SiC lower mold, (b) conventional-embossed, and (c) ultrasonic-assisted embossed PMMA replicas; (d) cross-sectional profiles of lower mold and PMMA replicas.

Each embossing experiment was conducted at 170 °C with a constant embossing speed of 0.06 mm/s and a maximum displacement of 1.20 mm. For conventional embossing (control group), no ultrasonic vibration was applied. In the ultrasonic-assisted embossing, longitudinal vibration, with frequency being 19.385 kHz and amplitude being 5.05 μm at 170 °C, was applied to the lower mold. After pressing, the PMMA preforms were held under a constant pressure of 100 N for 300 s, and then cooled to room temperature at a rate of 10 °C/s. Fig. 9b and c shows the embossed PMMA components, both exhibiting well-defined micro-protrusions with no noticeable distortion.

5.2 Experimental results

To investigate the effect of ultrasonic vibration on the PMMA's micro-filling capacity, the 3D surface morphologies of the microstructure lower mold and PMMA replicas were measured using an ultra-depth-of-field optical microscope (VHX-6000, Keyence Corp., Japan), as shown in Fig. 10a−c. It can be observed that the PMMA micro-protrusions formed by conventional embossing exhibit free-form curved tops (Fig. 10b), which is a typical phenomenon associated with incomplete filling.[36,37] In contrast, the PMMA micro-protrusions formed by ultrasonic-assisted embossing exhibit sharp-edged profiles (Fig. 10c), closely matching the bottom profile of the mold groove. Cross-sectional profiles of the lower mold and PMMA replicas were further measured for quantitative comparison (Fig. 10d). The profile of the ultrasonic-assisted embossed PMMA micro-protrusions demonstrates significantly better conformity to mold micro-grooves.

The average PMMA-to-mold filling ratio reaches 96.79% (calculated by the area ratio between each PMMA protrusion and mold groove), significantly higher than the 86.07% filling ratio in conventional embossing. This outcome confirms that ultrasonic vibration can significantly enhance the microscale filling capability of PMMA, consistent with the trend in ultrasonic-assisted molding of glass.[20,21]

6. Conclusion

This study presented the design of a novel Al_2O_3 (ceramic) ultrasonic horn, and validated its high-temperature vibration stability through numerical and experimental modal analyses. The practical performance of the Al_2O_3 horn under high-temperature and high-electromagnetic conditions was demonstrated through ultrasonic-assisted micro-embossing of PMMA under microwave heating. Conclusions of this study are as follows:

Numerical modal analysis indicated that as the terminal temperature increased form 25 °C to 800 °C, the longitudinal eigenfrequency of the Al_2O_3 horn decreased by only 238 Hz, far lower than the 982-Hz drop in Ti-6Al-4V horn. This minimal frequency drift, attributed to the low thermal expansion and high specific heat capacity of Al_2O_3, forms the theoretical basis for enhanced thermal stability of the ultrasonic system.

Experimental modal analysis demonstrated the overall stability of vibration frequency and amplitude of the Al_2O_3 horn across a wide temperature range (25−800 °C). This thermal stability ensures sustained resonance tuning, yielding a high mechanical quality factor (Q_m = 2135) at elevated temperatures—a critical advantage for high-temperature applications.

Ultrasonic-assisted embossing using the designed Al_2O_3 horn successfully replicated high-aspect-ratio, well-defined micro-protrusions on PMMA. The average filling ratio reached 96.79%, representing a 10.72% improvement over conventional embossing. This outcome highlights the unique advantage of ceramic horns in advanced micro-forming processes involving electromagnetic-thermal-mechanical fields, which is unattainable with conventional metallic horns.

In summary, the designed Al_2O_3 horn in this study can circumvent the limitations of conventional metallic horns, offering an innovative solution for ultrasonic applications under extreme conditions such as exposure to high temperatures or electromagnetic fields. Nevertheless, a key challenge lies in the inherent brittleness of ceramics,[38] which can limit the fatigue life and reliability of ultrasonic horns under high-amplitude vibrations. Additionally, the relatively low acoustic impedance of the Al_2O_3 horn may result in energy reflection losses when coupled with high-impedance terminal tools,[39] such as cemented carbides or carbon steels. Therefore, future efforts will focus on exploring toughened or flexible ceramic composites,[40] as well as functionally graded materials (FGMs),[41] to maintain both fracture toughness and acoustic transmission efficiency of ceramic horns.

Acknowledgments

This work was supported by the National Natural Science Foundation of China (No. 52205508), National Key Research and Development Program of China (No. 2022YFD2202103), Natural Science Foundation of Hunan Province (Nos. 2022JJ40876 and 2023JJ30147), and Changsha Municipal Natural Science Foundation (No. kq2202289).

Conflict of Interest

There is no conflict of interest.

Supporting Information

Applicable.

CRediT Statement

Hong Luo: Conceptualization, Formal analysis, Investigation, Project administration, Supervision, Writing – Original draft, Review and editing. **Haitao Zhao:** Conceptualization, Data Curation, Investigation, Methodology, Writing – Original draft, Review and editing. **Xianglong Yang:** Investigation, Data Curation, Formal analysis, Visualization. **Shuai Ma:** Data Curation, Validation. **Xinran Dong:** Formal analysis, Validation. **Qingyi Yang:** Data Curation, Formal analysis, Validation. **Yang Liu:** Data Curation, Validation. **Zhen Yin:** Investigation, Formal analysis, Methodology, Validation, Review and editing.

References

[1] A. Li, R. Jiang, R. Li, A. Fu, L. Zhang, L. Zhang, Effect of low-intensity ultrasound on grain refinement and heterogeneous nucleation mechanism of 2219 Al alloy, *Ultrasonics Sonochemistry*, 2025, **117**, 107341, doi: 10.1016/j.ultsonch.2025.107341.

[2] U. Zhapbasbayev, Z. Sattinova, G. Ramazanova, Simulation of hot casting shrinkage of thermoplastic beryllium oxide slurries with ultrasonic activation, *Engineered Science*, 2024, **32**, 1294, doi: 10.30919/es1294.

[3] D. Zhang, J. Sun, L. J. Lee, J. M. Castro, Overview of ultrasonic assisted manufacturing multifunctional carbon nanotube nanopaper based polymer nanocomposites, *Engineered Science*, 2020, **10**, 1002, doi: 10.30919/es5e1002.

[4] F. Thul, M. Liesegang, Estimation of wear behaviour for structures of ultrasonic welding sonotrodes by finite element simulations, *Wear*, 2025, **570**, 205973, doi: 10.1016/j.wear.2025.205973.

[5] Z. Yin, C. Dai, Z. Cao, W. Li, Z. Chen, C. Li, Modal analysis and moving performance of a single-mode linear ultrasonic motor, *Ultrasonics*, 2020, **108**, 106216, doi: 10.1016/j.ultras.2020.106216.

[6] J. Yu, H. Luo, T. V. Nguyen, L. Huang, B. Liu, Y. Zhang, Eigenfrequency characterization and tuning of Ti-6Al-4V ultrasonic horn at high temperatures for glass molding, *Ultrasonics*, 2020, **101**, 106002, doi: 10.1016/j.ultras.2019.106002.

[7] M. Roopa Rani, K. Prakasan, R. Rudramoorthy, Studies on thermo-elastic heating of horns used in ultrasonic plastic welding, *Ultrasonics*, 2015, **55**, 123-132, doi: 10.1016/j.ultras.2014.07.005.

[8] R. D. Kumar, M. R. Rani, S. Elangovan, Design and analysis of slotted horn for ultrasonic plastic welding, *Applied Mechanics and Materials*, 2014, **592-594**, 859-863, doi: 10.4028/www.scientific.net/amm.592-594.859.

[9] Y.-P. Tsai, J.-C. Hung, L.-C. Yin, C. Hung, Ultrasonic vibration-assisted optical glass hot embossing process, *The International Journal of Advanced Manufacturing Technology*, 2012, **60**, 1207-1213, doi: 10.1007/s00170-011-3669-8.

[10] Z. Liu, X. Jin, J. Zhang, Z. Hao, J. Li, Design optimization and eigenfrequency tuning of ultrasonic oscillator of one-dimensional longitudinal vibration at high temperature for laser welding, *The International Journal of Advanced Manufacturing Technology*, 2022, **119**, 4011-4029, doi: 10.1007/s00170-021-08530-0.

[11] W. Jung, J. Ra, K. Park, Design optimization of ultrasonic horn for micro-pattern replication, *International Journal of Precision Engineering and Manufacturing*, 2012, **13**, 2195-2201, doi: 10.1007/s12541-012-0291-0.

[12] Z. Wei, J. A. Kosterman, R. Xiao, G.-Y. Pee, M. Cai, L. K. Weavers, Designing and characterizing a multi-stepped ultrasonic horn for enhanced sonochemical performance, *Ultrasonics Sonochemistry*, 2015, **27**, 325-333, doi: 10.1016/j.ultsonch.2015.05.013.

[13] M. Roopa Rani, R. Rudramoorthy, Computational modeling and experimental studies of the dynamic performance of ultrasonic horn profiles used in plastic welding, *Ultrasonics*, 2013, **53**, 763-772, doi: 10.1016/j.ultras.2012.11.003.

[14] K. Anand, S. Elangovan, Design optimization of block horn for ultrasonic joining application using RSM–FEA–GA integration approach, *Proceedings of the Institution of Mechanical Engineers, Part E: Journal of Process Mechanical Engineering*, 2023, **237**, 2429-2439, doi: 10.1177/09544089221136801.

[15] W. Song, X. Yuan, S. Yu, X. Yu, A novel design of piezoelectric ultrasonic transducer with high temperature resistance, *International Ultrasonics Symposium*, October 22-25, Kobe, Japan, IEEE, 2018, 1-9, doi: 10.1109/ULTSYM.2018.8579785.

[16] M. U. Rehman, A. Xie, A. Rahman, Y. Zhang, A. Tian, X. Jiang, X. Xie, C. Zhou, T. Li, L. Liu, X. Gao, X. Er, R. Zuo, Enhanced energy storage performance with excellent thermal stability of BNT-based ceramics *via* the multiphase engineering strategy for pulsed power capacitor, *Journal of Materials Chemistry C*, 2025, **13**, 1395-1407, doi: 10.1039/D4TC04170D.

[17] J. Li, T. Momono, Effect of distribution coefficient K_0On the structure of ultrasonic ingots during solidification of aluminium alloys, *Materials Technology*, 2005, **20**, 202-207, doi: 10.1080/10667857.2005.11753138.

[18] K. Matsuda, T. Takehara, M. Yang, H. Uno, T. Kubo, G. Miyano, M. Yoshida, Verification of the mechanism of grain refinement by ultrasonic treatment of aluminum-4 wt pct silicon molten alloy, *Metallurgical and Materials Transactions A*, 2016, **47**, 2509-2516, doi: 10.1007/s11661-016-3377-y.

[19] K.-R. Deibel, K. Wegener, Methodology for shape optimization of ultrasonic amplifier using genetic algorithms and simplex method, *Journal of Manufacturing Systems*, 2013, **32**, 523-528, doi: 10.1016/j.jmsy.2013.05.010.

[20] J.-C. Hung, Y.-P. Tsai, C. Hung, Development of a new apparatus for ultrasonic vibration-assisted glass hot embossing process, *Precision Engineering*, 2013, **37**, 222-227, doi: 10.1016/j.precisioneng.2012.06.002.

[21] H. Luo, J. Yu, H. Lou, K. Huang, J. Hu, B. Xu, Thermal/tribological effects of superimposed ultrasonic vibration on viscoelastic responses and mold-filling capacity of optical glass: a comparative study, *Ultrasonics*, 2020, **108**, 106234, doi: 10.1016/j.ultras.2020.106234.

[22] E. Sahinoglu, T. Uslu, Effects of various parameters on ultrasonic comminution of coal in water media, *Fuel Processing Technology*, 2015, **137**, 48-54, doi: 10.1016/j.fuproc.2015.03.028.

[23] COMSOL Material Library. www.comsol.com. Comsol AB, Stockholm, Sweden, 2024.

[24] Y. Saotome, K. Imai, N. Sawanobori, Microformability of optical glasses for precision molding, *Journal of Materials Processing Technology*, 2003, **140**, 379-384, doi: 10.1016/S0924-0136(03)00828-8.

[25] I.-C. Rosca, M.-I. Pop, N. Cretu, Experimental and numerical study on an ultrasonic horn with shape designed with an optimization algorithm, *Applied Acoustics*, 2015, **95**, 60-69, doi: 10.1016/j.apacoust.2015.02.009.

[26] Z. Yang, L. Xu, H. Zhang, T. Gong, Z. Liang, L. Yao, Study on the nonlinear characteristic of a longitudinal piezoelectric ultrasound transducer with stepped horn, *Ultrasonics Sonochemistry*, 2025, **121**, 107533, doi: 10.1016/j.ultsonch.2025.107533.

[27] K.-B. Kim, D. K. Hsu, B. Ahn, Y.-G. Kim, D. J. Barnard, Fabrication and comparison of PMN-PT single crystal, PZT and PZT-based 1-3 composite ultrasonic transducers for NDE applications, *Ultrasonics*, 2010, **50**, 790-797, doi: 10.1016/j.ultras.2010.04.001.

[28] Y. He, T. Zhou, X. Dong, P. Liu, W. Zhao, X. Wang, Y. Hu, J. Yan, Generation of high-saturation two-level iridescent structures by vibration-assisted fly cutting, *Materials & Design*, 2020, **193**, 108839, doi: 10.1016/j.matdes.2020.108839.

[29] H. Mekaru, M. Takahashi, Frequency and amplitude dependences of molding accuracy in ultrasonic nanoimprint technology, *Journal of Micromechanics and Microengineering*, 2009, **19**, 125026, doi: 10.1088/0960-1317/19/12/125026.

[30] Y. Ben-Shimon, S. K. Reddy, A. Ya'akobovitz, Graphene foam resonators: fabrication and characterization, *Nano Research*, 2022, **15**, 225-229, doi: 10.1007/s12274-021-3463-3.

[31] X. Chen, J. Tang, W. Shao, B. Hu, J. Ye, An analytical and

experimental study on cutting characteristics and transient cutting force modeling in feed directional ultrasonic vibration-assisted cutting of high strength alloys, *Materials*, 2022, **15**, 7388, doi: 10.3390/ma15207388.

[32] H. Zhang, X. Gao, X. Liu, J. Wu, Calculation model for the steady-state vibration amplitude of a new type of cascaded composite structure-based ultrasonic transducer, *Nanomanufacturing and Metrology*, 2023, **6**, 27, doi: 10.1007/s41871-023-00204-7.

[33] J. Ju, Z. Long, S. Ye, Y. Liu, H. Zhao, Design of a novel integrated ultrasonic tool holder for friction stir welding, *The International Journal of Advanced Manufacturing Technology*, 2022, **120**, 5921-5932, doi: 10.1007/s00170-022-09136-w.

[34] E. Li, H. Kakemoto, T. Hoshina, T. Tsurumi, A shear-mode ultrasonic motor using potassium sodium niobate-based ceramics with high mechanical quality factor, *Japanese Journal of Applied Physics*, 2008, **47**, 7702, doi: 10.1143/jjap.47.7702.

[35] H. Luo, Y. Zhang, J. Yu, J. Qian, Q. Li, J.-A. Liu, Y. Zhang, K. Liao, Microwave-enabled rapid volumetric heating of moldable low-dielectric-loss glass, *Case Studies in Thermal Engineering*, 2024, **57**, 104364, doi: 10.1016/j.csite.2024.104364.

[36] H. Luo, J. Yu, J. Hu, K. Tang, B. Xu, F. Wang, Effects of uniform/nonuniform interface friction on mold-filling behavior of glass microarray: a numerical-experimental study, *Tribology Letters*, 2022, **70**, 20, doi: 10.1007/s11249-022-01563-w.

[37] K. Li, K. Jiang, G. Xu, X. Liu, F. Gong, Experimental and simulated analysis of glass deformation and filling modes during partial-filling hot embossing process, *Ceramics International*, 2020, **46**, 8059-8067, doi: 10.1016/j.ceramint.2019.12.031.

[38] O. Gavalda-Diaz, E. Saiz, J. Chevalier, F. Bouville, Toughening of ceramics and ceramic composites through microstructure engineering: a review, *International Materials Reviews*, 2025, **70**, 3-30, doi: 10.1177/09506608241308337.

[39] X. Qi, P. Ren, X. Tong, W. Qiao, Y. Shi, L. Bian, Z. Liu, X. Wang, Simultaneous regulation of piezoelectric performance and its temperature stability *via* the construction of multiscale heterostructures in KNN-based ceramics, *Chemical Engineering Journal*, 2025, **524**, 168277, doi: 10.1016/j.cej.2025.168277.

[40] J. Li, X. Wang, S. Guo, D. Zhang, J. Qi, Y. Wang, Recent progress in the fabrication strategies and toughening mechanism of flexible ceramics and their applications, *Journal of Materials Chemistry C*, 2024, **12**, 17742-17788, doi: 10.1039/D4TC01283F.

[41] S. Shetty, P. Numkiatsakul, K. Wickline, R. Incarnato, H. Wang, H. Kunkel, C. A. Randall, S. Trolier-McKinstry, Development of polymer-ceramic-metal graded acoustic matching layers *via* cold sintering, *IEEE Transactions on Ultrasonics, Ferroelectrics, and Frequency Control*, 2022, **69**, 1413-1427, doi: 10.1109/TUFFC.2022.3148792.

Publisher's Note: Engineered Science Publisher remains neutral with regard to jurisdictional claims in published maps and institutional affiliations.

Open Access